MODEL DRIVEN QUANTIFICATION OF INDIVIDUAL AND COLLECTIVE CELL MIGRATION

Caroline Rosello[1], Pascal Ballet[2], Emmanuelle Planus[1] and Philippe Tracqui[1,3]

[1]CNRS, Laboratoire TIMC-IMAG, Equipe DynaCell, Institut de l'Ingénierie et de l'Information de Santé (In[3]S), Faculté de Médecine, F-38706 La Tronche Cedex, France.
[2]Département Informatique, EA 2215, Université de Bretagne Occidentale, BP 809, F-29285 Brest Cedex, France.
[3]Author for correspondence: Dr. Ph Tracqui, Laboratoire TIMC-IMAG, Equipe DynaCell, Institut de l'Ingénierie et de l'Information de Santé (In[3]S), 38706 La Tronche Cedex, France. Email: Philippe.Tracqui@imag.fr

ABSTRACT

While the control of cell migration by biochemical and biophysical factors is largely documented, a precise quantification of cell migration parameters in different experimental contexts is still questionable. Indeed, these phenomenological parameters can be evaluated from data obtained either at the cell population level or at the individual cell level. However, the range within which both characterizations of cell migration are equivalent remains unclear. We analyse here to which extent both sources of data could be integrated within a unified description of cell migration by considering the motility of the endothelial cell line EAhy926. Using time-lapse video-microscopy and associated analysis of digital image time series, we quantified EAhy926 random motility coefficient, migration speed and trajectory persistence time in two different migration assays: the in vitro wound healing assay, and the cell-populated agarose drop assay. In order to analyse the agreement between independent quantifications of cell motility based either on individual cell analysis or cell population dynamic analysis, a theoretical multi-agents cellular model was developed and discussed as a possible theoretical framework able to unify these multi-scale data. Model simulations especially reveal the potential bias induced by cell proliferation and cell-cell adhesion when cell migration parameters are estimated from the extensively used in vitro wound healing assay.

Keywords: random walk model, multi-agents model, wound healing assay, multi-scale quantification, agarose drop migration assay.

1. INTRODUCTION

Migration of mammalian tissue cells plays an important role in fundamental physio-pathological processes, including wound repair and angiogenesis (Manes *et al.*, 2000; Lauffenburger and Griffith, 2001; Ingber, 2002). In these contexts, the motile behaviour of endothelial cells is a key factor for the development of the capillaries network that occurs during vascular remodelling after injury or when tumour vascularisation takes place (Benndorf *et al.*, 2003).

Acta Biotheoretica **52:** 343–363, 2004.

Using migration assays like Boyden chambers (Boyden, 1962) gives little information on the spatio-temporal evolution of the cell motility over a 2D substrate. Thus, quantification of the motile behaviour of cells relies mostly on time-lapse video-microscopy, which on the other hand produces a huge amount of rough data (Soll and Voss, 1999). Consequently, the quantification of the motile behaviour of cells relies not only on the choice of relevant experimental models, but also critically on the analysis of the so-obtained data by relevant mathematical models (Maheshwari and Lauffenburger, 1998). On the experimental side, the *in vitro* wound healing (IWH) assay is extensively used for the characterization and the quantification of collective cell motility. In this assay, a confluent cell monolayer is gently wounded by a pipette tip whose size determines the wound geometry. More recently, the cell-populated agarose drop (CPAD) assay has been used as an experimental model for characterizing the motility of cell on various extracellular substrates (Planus *et al.*, 1999). In this assay, cells are initially trapped within an agarose drop and then diffuse progressively out of the drop onto the surrounding extracellular substrate. Contrary to the IWH assay, where the wound size determines possible influence of the opposite wound margins, the CPAD assay can be viewed as an open wound. In both assays, data analysis can be undertaken either at the cell population level or by gathering information obtained at the individual cell level. In the IWH assay, apparent cell motility can be globally quantified from the decrease with time of the wounded area, while in the CPAD assay, cell motility is globally characterized by the wave-like propagation of the migrating front of cells moving outside the drop. Quantification of intrinsic cell motility from individual trajectories gives more precise information, but at the price of a larger variability. Indeed, cells appear to move along fairly linear paths over short time intervals but can follow more randomly oriented directions over longer time intervals. Cell trajectories can then be analysed in the framework of persistent random walk models (DiMilla *et al.*, 1992), which consider mean cell velocity and persistence time as two basic phenomenological parameters for the characterization of cell motility.

In this paper, a comparison between cell motility quantification obtained from the global and the local cell migration analysis is undertaken for the permanent endothelial cell line EAhy926 (Edgell *et al.*, 1983; Bouis *et al.*, 2001), derived from human umbilical vein endothelial cells (HUVEC). As HUVEC, these cells are able to form capillary-like structures when cultured on extracellular matrices like matrigel or fibrin gels (Vailhé *et al.*, 1997; Tranqui and Tracqui, 2000) and are thus of special interest for the study of angiogenesis or wound healing. In the first part of the results section, the migration of EAhy926 cells is quantified in both IWH and CPAD assays. However, we can anticipate from other experimental results that potential bias could give rise to different results between the global and the local approaches. Indeed, *in vitro* studies of epithelial monolayer wounds showed that wound closure is not only achieved by the motion of cells at the wound margins, but also involves the dynamics of the four or five rows of cells behind the margins (Klepeis *et al.*, 2001). Moreover, the repair capacities of a wounded tissue also involve a series of other processes such as proliferation, cell-cell adhesion or migration induction by biochemical signalling pathways (Fenteany *et al.*, 2000).

In the second part of the results section, a theoretical approach, based on the formulation of a multi-agents cellular model, is developed in order to address the

relationships between intrinsic and apparent cell motility, defined as the integrated cell behaviour resulting from additional environmental clues and other cell-cell dynamical interactions. In this model, each cell is considered as an agent characterized by intrinsic structural and dynamical properties. Furthermore, each cell-agent interacts, through a bi-directional signalling process, with its environment, including other cells. Simulations of the multi-agents model have been performed when considering both the spatial constraints induced by the different geometries of the migration assays considered here, as well as different intrinsic motility, proliferative and adhesive properties of individual cells. In the light of these simulation results, we discussed the extent to which global estimation of cell motility can be considered as the integration of all the individual cell trajectories tracked at the individual cell level.

2. MATERIALS AND METHODS

Cell culture

Experiments were performed using the human permanent endothelial EAhy926 cell line. This cell line is derived from the fusion of HUVEC with the A549 human lung epithelial carcinoma cell line (Edgell *et al.*, 1983). Cells were grown in a complete medium composed of Dulbecco's Modified Eagle Medium supplemented with 2-mM glutamine, 10% heat-inactivated foetal calf serum (Invitrogen, Life Technologies) and penicillin-streptomycin (Life-Technologies) in a cell culture flask at 37°C in a humidified CO_2 (5%) atmosphere. Cells were sub-cultured using trypsin/EDTA mixed solution to detach adherent cells from the culture flask and then seeded at 15000 cells/cm^2 in complete medium.

In vitro wound healing (IWH) assay

The IWH assay was carried out as previously described (Ronot *et al.*, 2000). Cells were cultured until confluence (10^5 cells/cm^2) in glass culture chambers (LabTech, Nunc). Cell monolayers were gently scratched with a pipette tip, creating a rectangular wound between 200 and 500 μm width, and extensively rinsed with PBS without calcium and magnesium (Life Technologies) to remove all cellular debris. Fresh complete medium was then added. The subsequent colonization of the denuded surface was quantified by time-lapse video-microscopy over 24 to 48 hours (see below).

Cell populated agarose drop (CPAD) assay

This cell migration assay was derived from the method described by Varani and Ward (1978) and adapted from Kiernan and Ffrench-Constant (1993). EAhy926 cells were suspended at 20x10^6 cells/mL in complete medium supplemented with 0.3% agarose and maintained at 37°C to prevent gelling of the agarose. Drops of 2 μL volume were taken from this cellular suspension and plated in the centre of fibrin gels previously prepared in Petri culture dishes (see below). The preparation was placed at 4°C for 15 minutes to allow the agarose to turn into gel. Then, 0.5% foetal calf serum serum (Invitrogen, Life Technologies) supplemented medium was added to cover the

drop. Cell migration was then recorded by digital time-lapse video-microscopy during 24 to 48 hours.

Preparation of fibrin gels

Inside a 35 mm diameter culture Petri dish, 1 mm thickness gels were prepared from a PBS buffer (Life Technologies), free of calcium and magnesium and containing fibrinogen (1 mg/mL, Sigma-Aldrich), thrombin (0.4 U/mL, Sigma-Aldrich) and aprotinin (5 μg/mL, Roche Diagnostics), a plasmin inhibitor. Gels were then incubated over night at 37°C in a humidified atmosphere.

Cell proliferation assay

Cells were seeded at 15000 cells/cm^2 in complete medium inside 35 mm diameter culture dishes and incubated at 37°C in a humidified and CO_2 regulated (5%) atmosphere. The evolution of cell density with time was followed over seven days by cell counting at successive time intervals. Cell cultures were gently rinsed out and then incubated with trypsin/EDTA mixed solution until cells detached. Cell density was determined manually with a Malassez counting hemocytometer.

Time-lapse video-microscopy

For each experiment, culture dishes with migrating cells were placed on the stage of a Zeiss Axiovert 135M inverted microscope equipped with a Phase 1 Achrostigmat 5x or x10 objective, a temperature and CO_2 controlled chamber (37°C, CO_2 5%, humid atmosphere) (M Incubator, Carl-Zeiss), automated shutters (Uniblitz) and a CCD camera (CoolSNAP, Roper Scientific) monitored via a computer by an image acquisition and analysis software (MetaVue, Roper Scientific). The microscope calibration was performed using a micrometric slide (PRESS-PRO21). Scaling along x and y axes with x5 objective were respectively of 0.833 μm/pixel and 0.909 μm/pixel. To observe significant cell movement during the time course of each experiment, video-microscopy images were continuously recorded for 24 or 48 hours, with a sampling period of 1 h for IWH assays and 0.5 h for CPAD assays.

Cell migration analysis at the cell population level

The MetaVue software (Roper Scientific) was used for the image analysis of video-microscopy sequences recorded for each assay. In the IWH assay, the wounded surface $A(t_n)$ at each time interval t_n was obtained by image segmentation. The mean wound closure velocity $V(t_n)$ in the direction perpendicular to the initial wound margins (Figure 1) was inferred from a least-square regression applied within a sliding window in time including k experimental points $A(t_i)$ according to the relationship:

$$-V(t_n) = \frac{k.\sum_i \left(t_i\,.A(t_i)\right) - \sum_i \left(t_i\right)\sum_i \left(A(t_i)\right)}{H.\left(k.\sum_i \left(t_i^2\right) - \left(\sum_i \left(t_i\right)\right)^2\right)}, \quad i = n - \frac{(k-1)}{2}, \ldots\ldots, n + \frac{(k-1)}{2}$$

where H is the constant height of the wounded area. We took a sliding window width given by $k = 5$. In the CPAD assay, the segmentation procedure gives, at each time interval, the surface of the 2D domain extending from the agarose drop boundary up to the roughly circular line defining the migration front determined by the leading migrating cells. The mean velocity of the cell population $V(t_n)$ is again approximated by a linear regression over the experimental points.

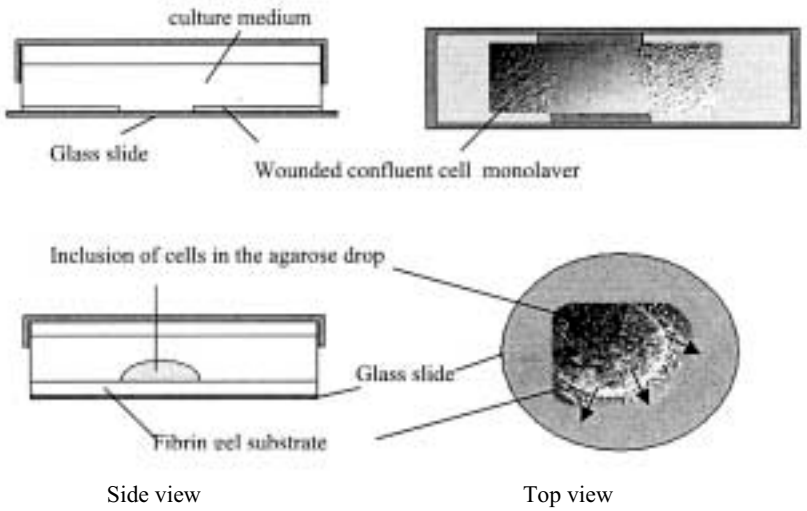

Figure 1. Schematic views and video-microscopy phase contrast images of the two cell migration assays. A: In the *in vitro* wound healing (IWH) assay, a confluent cell monolayer is wounded. B: In the cell-populated agarose drop (CPAD) assay, cells initially confined within an agarose drop escaped from it and moved centrifugally on the underlying fibrin gel.

Cell migration analysis at the individual cell level

In both types of migration assays, individual paths of 30 cells were tracked semi-automatically with the image analysis software TrackImageBio (ORME, Toulouse). At each time $t_n = n.\Delta t$, where Δt is the sampling time interval, the position of each cell centroid $\{x(t_n),y(t_n)\}$ was recorded. A quantitative characterization of each cell migration is then inferred from these data by considering the individual cell trajectory as a persistent random walk. In this modelling approach, the squared displacement $d.d(t_n,i\,\Delta t)$ of each cell is computed, over a time period $[i.\Delta t]$, from the distance between the successive positions $\{x(t_n),y(t_n)\}$ and $\{x(t_{n+i}\,\Delta t),y(t_{n+i}\,\Delta t)\}$:

$$d.d(t_n,i\,\Delta t) = [(x(t_{n+i}\,\Delta t) - x(t_n))^2 + (y(t_{n+i}\,\Delta t) - y(t_n))^2]. \quad (1)$$

Then, the mean-squared displacement $<d.d(t_k)>$ for a given time $t_k = k.\Delta t$ is obtained by averaging all the distances computed from overlapping intervals of width k moving over all cell positions, from the initial time t_0 up to the final observation time $t_{end} = N.\Delta t$. Application of this iterative procedure gives:

$$< d.d(t_k) > \; = \frac{1}{(N-k+1)} \sum_{i=0}^{N-k} d.d(t_i, k\Delta t). \qquad (2)$$

Variances in squared displacements are given in a similar way, for $k < N$, by:

$$\sigma^2_{d.d}(t_k) = \frac{1}{(N-k)} \sum_{i=0}^{N-k} \left[d.d(t_i, k\Delta t) - < d.d(t_k) > \right]^2. \qquad (3)$$

Different theoretical approaches have shown that the mean squared displacement $< d.d >$ over time t of a cell moving in an isotropic environment can be characterized by only two parameters, cell speed V and persistence time P, according to the analytical expression (DiMilla *et al.*, 1992):

$$< d.d(t) > \; = 2.\, V^2.P.[t - P.(1 - \exp(-t/P))]. \qquad (4)$$

Based on this relationship, a non-linear least squares fitting procedure has been used to identify from each cell trajectory a parameter set (Vi,Pi).

Let us remark that at very short time intervals, the cell centroid motion is rather uncertain. Moreover, in the overlapping procedure, averaging could be highly biased by an insufficient number of intervals if the width k is too large. Thus, mean squared displacement computed for time intervals less than $t_{min} = 4.dt$ or greater than $t_d = t_{end}/2$ were not included in the fitting procedure. To avoid the bias induced by the sampling interval used for image acquisition as well as the bias induced by almost immotile cells, cells with identified persistence times P less than 1 h and greater than $t_{end}/3$ were excluded from further analysis. To evaluate the significance between results, Student t-tests were performed with significance levels set at $p < 0.05$.

3. RESULTS

Individual cell tracking

The so-called wind roses representations were used to gather the individual cells trajectories recorded by video-microscopy in both migration assays (Figure 2). These diagrams are obtained by translating all trajectories in such a way that each initial cell position coincides with the axes origin. Both diagrams in Figure 2 show that cells follow oriented trajectories. In the IWH assay (Figure 2A), cells move from the wound margins toward the centre of the denuded area, i.e. from left to right (positive x abscissa values) or from right to left (negative x abscissa values). In the CPAD assay (Figure 2B), one observes as expected a centrifugal motion of the cells over the fibrin gel, away from the upper left region occupied by the agarose drop (Figure 1).

To go beyond this qualitative aspect of individual cell migration, identification of the two phenomenological parameters, cell speed V and persistence time P, was undertaken as described in Section 2. Figure 3 exemplifies that for quite different cell trajectories (left column, Figure 3), a very satisfactory goodness of fit was obtained with the persistent random walk model (right column, Figure 3).

A

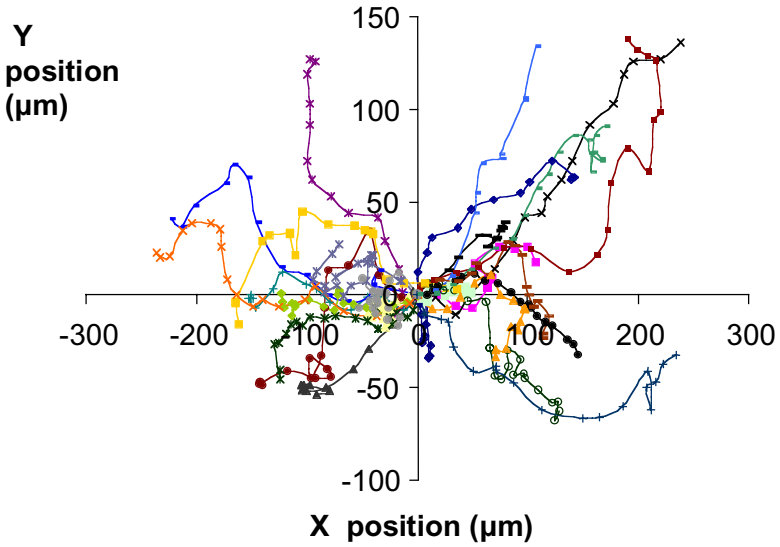

B

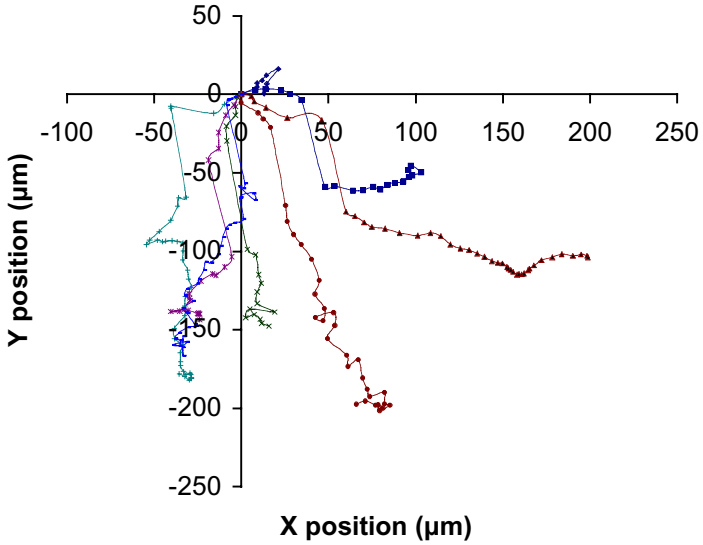

Figure 2. Individual cells trajectories tracked in both migration assays. A: Trajectories of 36 cells are compiled from three IWH assays. As expected, cells from the right wound margin migrate toward the wound centre, with a significant number of trajectories which are not perpendicular to the wound margin. Conversely, cells from the left wound margin move to the right. B: Trajectories of eight cells moving from the agarose drop in a CPAD assay. The drop located is in the upper left part of the graph. All cell trajectories have been translated such that the initial position of each cell coincides with the origin of the graph.

Mean values of cell speed and persistence time, identified from a total of 44 cell trajectories, are summarized in Table 1. Cell speeds and persistence times are in the order of 15 μm/h and 2.5 hours respectively in the IWH assays, with non-significant differences between the three IWH experiments. Similar values are obtained with the CPAD assays. One should however notice that this similarity corresponds to different experimental conditions: CPAD assays were conducted with low foetal calf serum concentration (0.5% FCS) to prevent fibrin gel proteolysis, while IWH experiments were performed with 10% FCS (see Section 2). In other words, cell migration and adhesion on a deformable extracellular matrix (CPAD) seems to counterbalance the decrease of cell motility induced by low FCS concentrations.

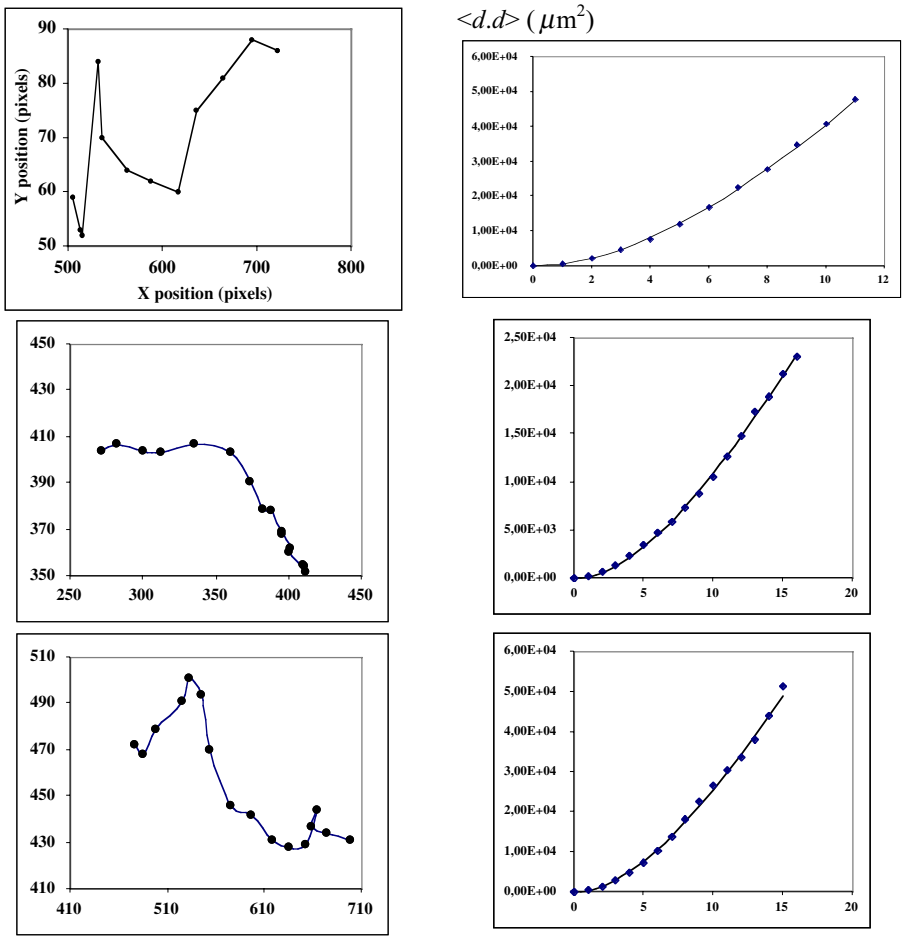

Figure 3. Identification of cell migratory parameters assuming that each cell follows a persistent random walk, exemplified by three typical cell trajectories (left part of the figure). The corresponding computed mean squared displacements are indicated on the right part of the figure. For each graph, the solid line corresponds to the best fit to the data for the analytical expression given by equation (4). Axes labels are the same for each column.

Table 1. Mean cell speed and mean persistence time determined from the fit to experimental trajectories of the indicated number of motile cells when using a persistent random walk model for cell movement in IWH and CPAD migration assays. Cell diffusivity coefficients were calculated from these mean values using equation (5).

Migration assay	Substrate	Nb cells	$V(\mu$m/h)	P(h)	$\mu(10^{-6}$cm^2/h)
IWH	Glass (# IWH 1)	14	15.50 ± 3.04	2.41 ± 0.69	2.90 ± 0.87
	Glass (# IWH 2)	11	13.94 ± 5.62	2.72 ± 0.64	2.64 ± 1.05
	Glass (# IWH 3)	11	15.25 ± 3.22	2.58 ± 0.85	3.00 ± 0.98
CPAD	Fibrin gel	8	14.86 ± 1.11	2.14 ± 0.63	2.37 ± 0.71

A theoretical link between individual cell migratory behaviour and cell migration at the cell population level is provided by computing the associated random motility coefficient (or cellular diffusion coefficient) μ from the V and P mean values, according to the relationship (DiMilla *et al.*, 1992):

$$\mu = \frac{P.(V)^2}{2} \tag{5}$$

where the factor 2 comes from the dimensionality of the 2D substrate. Over a long period of time, i.e. when $t >> P$, the cellular diffusion coefficient characterizes the linear variation with time of the mean squared displacement of a persistent random walker as a limit of equation (4), which reads in a 2D space:

$$< d.d(t) > = 4.\mu.[t - P]. \tag{6}$$

Random motility coefficients calculated in Table 1 are not statistically different based on a Students' t-test. In the IWH assays, the reported values of V and P are lower and larger, respectively, than those reported by Kouvroukoglou *et al.* (2000) for bovine pulmonary artery endothelial cells ($V = 40$ μm/h, $P = 0.4$ h). But from these latter values, these authors calculated a random motility coefficient of 3.5 10^{-6} cm^2/h which is close to the values reported in Table 1 for IWH assays. More generally, the relationship given by equation (6) provides a simple way to characterize the variation of random cell motility cell on different extracellular substrates (Kouvroukoglou *et al.* 2000; Tan *et al.*, 2001). But one can wonder if such a quantification of cell migration from individual cell trajectories is equivalent to a quantification obtained from measurements made at the cell population level.

Quantification of cell migration from global population analysis

According to the procedure given in Section 2, the evolution with time of the wounded area was determined by iterative image segmentation of the wound margins for each time-lapse video-microscopy sequence. In all experiments, wound closure occurs within 30 hours (Figure 4A-4B). Quantification of cell migration from the decrease of the wound area $A(t)$ has been extrapolated from equation (6) by considering the following analytical expression (with $t > P$):

$$A(t) = A_0 - 4.H\sqrt{\mu.(t - P)} \tag{7}$$

where H is the constant height of the wound area ($H = 943\ \mu$m).

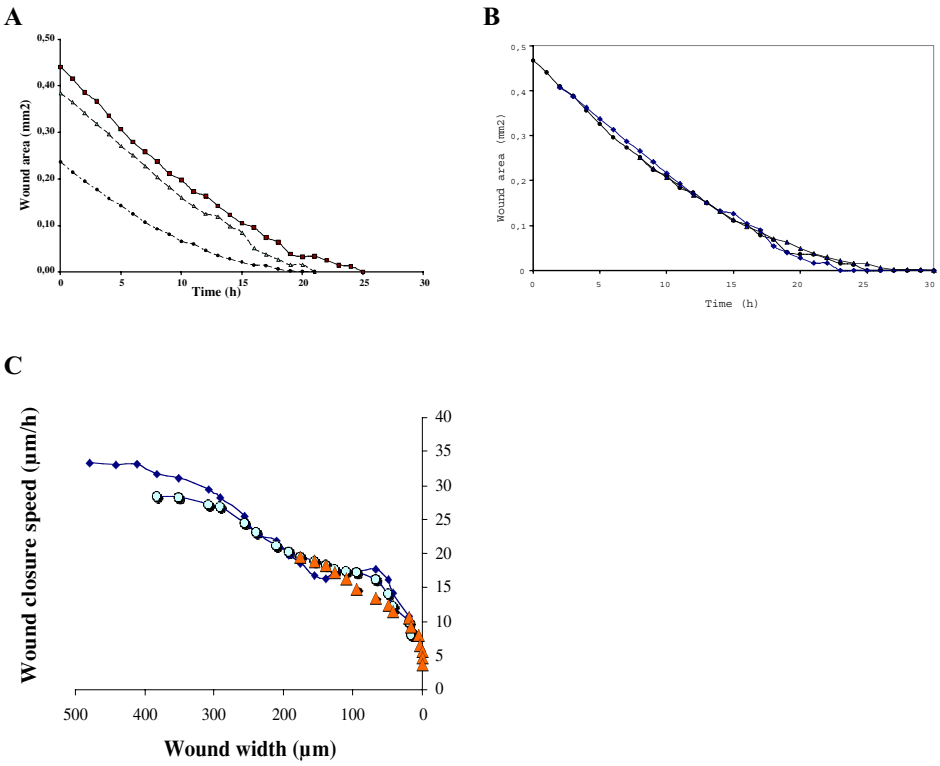

Figure 4. Evolution with time of the wounded area in three IWH assays. A: Experimental initial wound area is not the same in the three cases, which seems to give rise to different wound closure kinetics. B: When the initial wound areas of the two lowest curves are superimposed to the corresponding values taken on the upper curve after horizontal translation, the kinetics of wound closure appear to be very similar. C: The wound closure velocities computed from the slope of the above curves decrease significantly and in a non-linear way when the wound width falls below 100 μm.

A very satisfactory fit to the experimental data, corresponding to almost zero values of the mean least-squared criterion, has been obtained: this allows a reliable identification of the two parameters μ and P for each IWH migration assay. The values reported in Table 2 are quite coherent with those obtained from the fit to individual cell trajectories. However, this cell population approach gives larger values of the persistence time compared to the one obtained by applying a persistent random walk model for individual cell movement.

Table 2. Persistence time and cell diffusivity coefficient identified globally from the decrease of the wound area with time (Figure 4B). The estimated speed V of each wound margin in the first hours of wound healing is derived from the linear part of the wound area curve.

Migration assay	V(μm/h)	P(h)	$\mu(10^{-6}cm^2/h)$
IWH 1	10	2.34	2.48
IWH 2	14	3.38	5.98
IWH 3	17	3.07	6.48

Interestingly, even if the initial wounded areas are not the same, all the observed experimental curves obtained with IWH assays exhibit the same profile when initial wounded area values are rescaled by horizontal translation (Figure 4B). This highlights a possible regulation of the speed of wound closure, which progressively decreases up to a zero value but with a strong dependence on the wound width (Figure 4C). For large wounds (~400 μm width), wound closure speeds are roughly constant. From these quasi-constant values, an initial migration speed of the wound margins is estimated as half of this value, assuming symmetrical wound closure (Table 2). After this initial phase, wound closure speed decreases quite rapidly when the wound width falls below ~100 μm, i.e. about five cell length. Thus, direct cell-cell contacts do not appear as the leading factor of this regulation of wound closure speed. One can expect that such a regulation process is linked to the wound geometry, i.e. to the existence of two opposite margins of migrating cells. This means that in an open-wound geometry, like in the CPAD assay, the cell migration velocity would remain almost constant. This is indeed what we observed: the area bounded by the migrating front and the agarose drop border increases almost linearly, with an estimated slope of 11.6 μm/h (Figure 5).

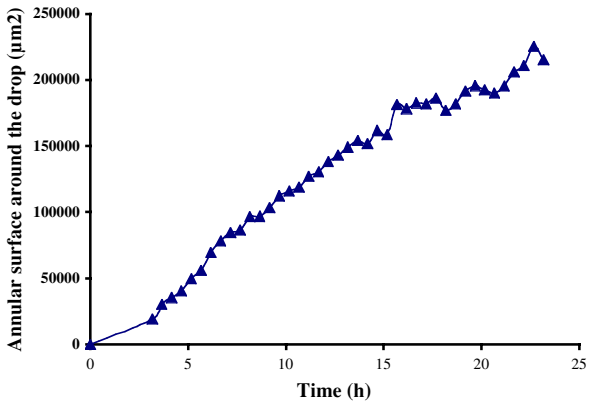

Figure 5. Evolution with time of the area bounded by the agarose drop on the inner part and by the front of the migrating cell on the outer part. This area is obtained by segmentation of the time-lapse video-microscopy images.

Comparison between isolated cells based quantification of cell migration and cell population based quantification of cell migration

Assuming a symmetrical wound closure, we estimated the theoretical time of closure T in IWH assays by making use of equation (4) and considering the time needed for each wound margin to travel a distance $L_0/2$, where L_0 is the initial wound size. We then get:

$$\left(\frac{L_0}{2}\right)^2 = 4.\mu.\left[T - P.(1 - e^{\frac{-T}{P}})\right]. \quad (8)$$

Considering that T is larger than the persistence time P, an estimated value of the time T needed for wound closure would be:

$$T = P + \frac{(L_0)^2}{16.\mu} \quad (9)$$

These predicted values are compiled and compared in Table 3 when considering the diffusivity coefficient, speed and persistence time derived, on one hand from individual cell trajectories (Table 1), and on the other hand, from cell population analysis (Table 2). Globally, the measured and the predicted times needed for wound closure are quite similar when predictions are made from global population analysis. Larger values of the measured time, as with experiment IWH 1, could be explained by the fact that the predicted time of closure assumes that cell migration occurs only along a direction perpendicular to the wound margins, while real cell trajectories are more random (Figure 2A).

Table 3. Comparison between theoretical times of wound closure predicted from individual cell approach parameters (Table 1) and global cell population approach parameters (Table 2).

Migration assay	Width L_0 (μm)	Measured time for wound closure (h)	Predicted time T from global approach (h)	Predicted time T from local approach (h)
IWH 1	251	21	18.2	16.0
IWH 2	407	20	20.7	41.9
IWH 3	467	24	24.1	48.0

Differences between measured and predicted times of wound closure appear significantly when predictions are made from the individual cell approach. Since predicted times are higher, one can then wonder how additional cellular factors, such as cell proliferation, may explain such differences (Zahm *et al.*, 1997). Indeed, within the confluent cell monolayer, proliferation may induce an increasing pressure which would enhance cell migration toward empty locations, while isolated cells in non confluent conditions do not undergo such mechanical stimulus. This analysis is undertaken in the next section by considering a multi-agent model, in which each cell behaves as a separate motile agent whose interactions with neighbouring cells determine the global population behaviour.

Migration assays simulations based on a multi-agents model

Among the various methods used for modelling biological processes, multi-agents systems (MAS) are of special interest since they explicitly relate the emergence of collective dynamical processes to the description of individual agent behaviour (Mansury and Deisboeck, 2003). If compared to classical cellular automaton approaches, MAS allow a more refined description of the local agent properties within a perception-decision-action scheme (Boucher *et al.*, 1998). Such an approach has been used here as an explicit means for analysing how individual cell properties determine the collective cell behaviour observed at a cell population scale in migration assays. Indeed, this approach provides a multi-scale framework in which integration of quantitative data characterizing individual cell behaviour (cell motility, cell division, cell-cell adhesion, ...) can be qualitatively and quantitatively compared to the data characterizing the morphological evolution with time of the cell monolayer, especially wound closure in IWH assays.

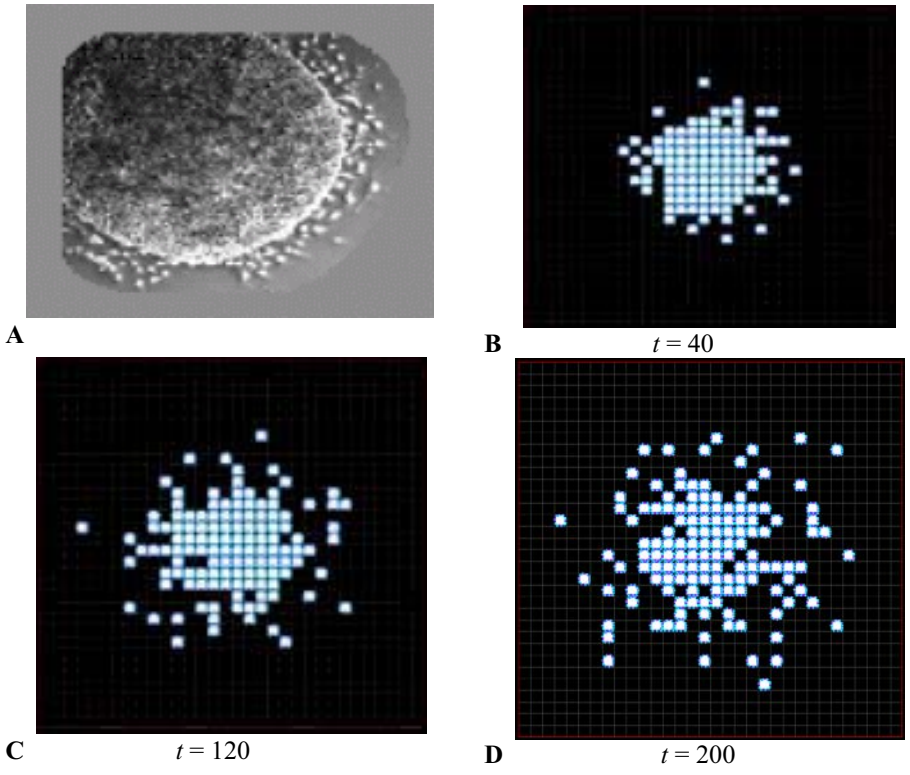

Figure 6. Simulated migration of cells in a CPAD assay without cell proliferation. A: Microscopic image of the agarose drop and of the first quasi-circular rows of migrating cells. B-D: Simulated radial migration of cells, away from the initial cell aggregate, with snapshots taken at successive times. The simulated cell migratory behaviour, composed of both random motion and radial displacement, depicts quite well the experimental cell migration observed in the CPAD assay, as exemplified by a comparison of Figures 6A and 6C.

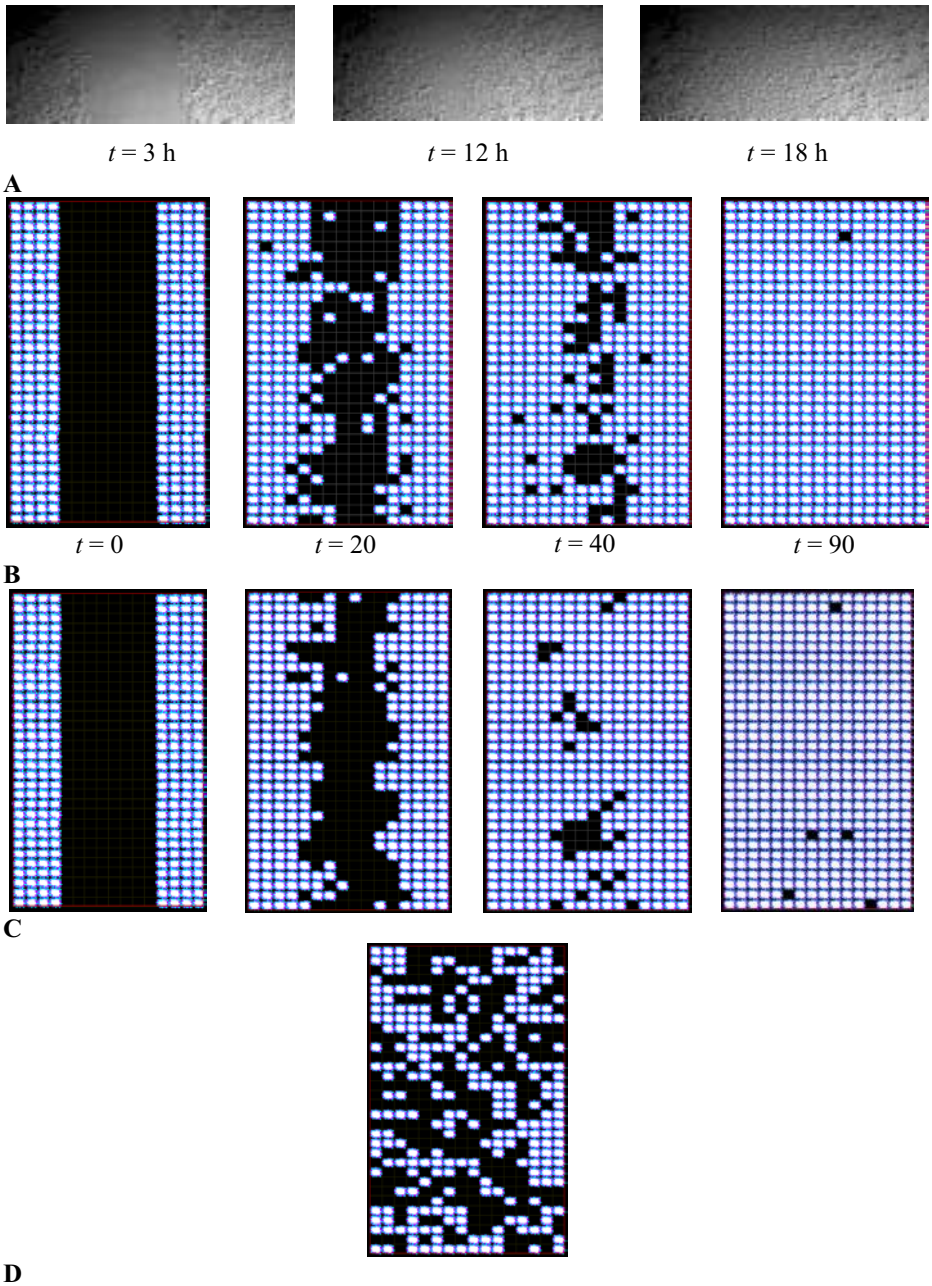

Figure 7. Snapshots of the video-microscopy sequence obtained during IWH assays (A) and simulated wound closure computed with the multi-agents model when considering: (B) cell-cell adhesion and cell proliferation, (C) no cell-cell adhesion and cell proliferation or (D) no adhesion and no proliferation.

The MAS has been developed here on a rectangular grid lattice spanning a two-dimensional space. Initial conditions are defined according to the specificity of the migration assays, i.e. a central rectangular region devoid of cells in the simulation of the IWH assay (Figure 7) or a central cluster of cells in the CPAD assay (Figure 6). The intrinsic features of the cell-agent regarding migration processes, proliferation and cell-cell interactions are defined by the following rules.

A cell is eligible to either migrate or proliferate according to the number of adjacent empty locations in its neighbourhood. The number of empty locations determines both the probability of mitosis and the probability of migration. These probabilities are additionally modulated by a mitosis factor mf ($0 \leq mf \leq 1$) and a migration factor df ($0 \leq df \leq 1$). Thus, a cell Cl residing in a given location (i,j) of the 2D grid may generate two daughter cells with the probability:

$$Pm\,(Cl_{i,j}) = mf.\,ESF_{i,j}\,. \tag{10}$$

The empty space factor $ESF_{i,j}$ is the ratio of the number of empty locations $Ne(Cl_{i,j})$ in the neighbourhood of the considered cell over the maximum number of empty locations, which gives in a 2D space:

$$ESF_{i,j} = \; ESF(Cl_{i,j}) = Ne(Cl_{i,j})/8. \tag{11}$$

In addition to the above features, cell-cell interactions and cell-substrate interactions are considered globally through an adhesion factor ad, with $0 \leq ad \leq 1$. If $ad = 1$, adhesion is maximum and the cell cannot move. Finally, the cell Cl may migrate according to the probability:

$$Pd\,(Cl_{i,j}) = df.\,(1 - ad).\,ESF_{i,j}\,. \tag{12}$$

During each elementary time step, each cell performs three successive steps:

(i) the examination of the neighbourhood of its current location and then the evaluation of the corresponding $ESF_{i,j}$ value;

(ii) the computation of the capability to proliferate or to migrate, depending on the mitosis, migration and adhesion factors;

(iii) the realization of the final dynamical action, based on a stochastic decision process. Two numbers $n1$ and $n2$ are randomly chosen and, according to these values, the cell $Cl_{i,j}$ will divide if $n1$ is smaller than $Pm\,(Cl_{i,j})$ and/or migrates if $n2$ is smaller than $Pd\,(Cl_{i,j})$.

In order to manage potential competition of two cells for the same location (when two cells tend to move toward the same location or to create daughter cells at the same site), each individual cell action is immediately taken into account by the other cells. For example, in the case of cell mitosis, the $ESF_{i,j}$ value is modified and the probability of migration changed accordingly.

Migration assays simulations

For given initial conditions (initial cell density, initial geometry of the cell cluster or cell monolayer) the dynamics of the overall cell population has been simulated for different values of the cell motility, proliferation rate and cell-cell adhesion.

Figure 6 shows the simulated wave-like propagation of the cells from the initial cell cluster in the CPAD assay. The centrifugal cell motion gives rise quite rapidly to a rather scattered spatial distribution of cells. The migrating front remains more coherent if cell proliferation occurs (data not shown).

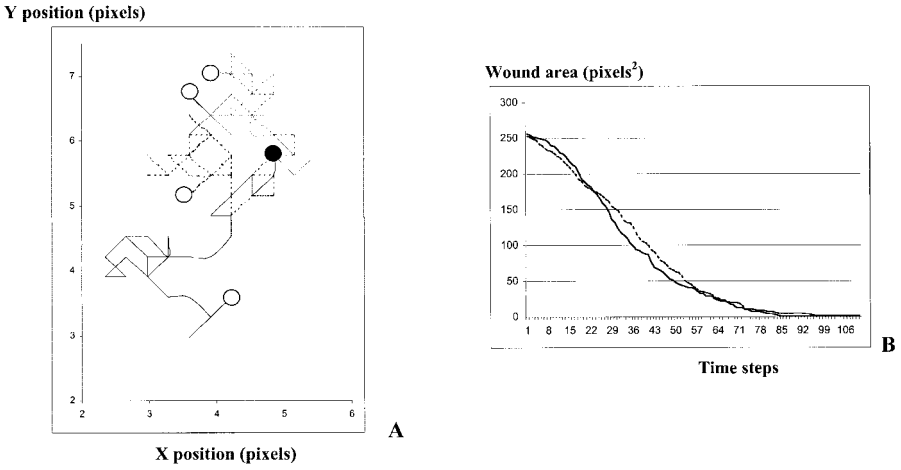

Figure 8. A: Computed individual cell trajectories given by the decision rules and properties of the multi-agent model in the simulation of an IWH assay. Black circles denote the initial cell position, while open circles indicate the final cell locations. B: Associated evolution of the wounded area without considering cell-cell adhesion (solid line) or when taking into account cell-cell adhesion (dotted line).

The simulated spatio-temporal dynamics of the wound closure in the IWH assay is shown in Figure 7B-7D. The grid consists of 32 rows and 16 columns, corresponding to a real wound portion of 640 μm x 320 μm, each cell-agent being of size 20 μm x 20 μm. At time zero, a rectangular wound of size 32 rows x 8 columns is realized in the modelled cell monolayer, each wound margin then including 128 cells.

For a migration factor of 0.3 (corresponding to a cell migration speed of 20 μm per time step) and considering a small proliferation rate by setting the mitosis factor to 0.1, wound closure is realized in 90 time units (Figure 7B and 7C). When cell-cell adhesion is considered, with adhesion factor set to 0.6, the wound closure appears slightly slower at intermediate times (t = 40, Figure 7B). The corresponding simulated individual trajectories of some cells taken at the right wound margin are shown in Figure 8A. These simulated paths look rather geometric but still similar to the persistent random walk motion of real cells exhibited in Figure 2A. Moreover, the associated decrease with time of the wound area (Figure 8B) is very similar to the experimental evolution reported in Figure 4A, with a progressive decrease of the wound closure speed at the end of the healing-like process.

In the above IWH assay simulations, a weak cell proliferation has been considered. Indeed, without proliferation, the spatio-temporal evolution of the wound closure is very irregular: the wound geometry disappears and cells are just redistributed over the 2D grid (Figure 7D).

For each simulation, the increase with time of the cell number can be determined easily (Figure 9A). This simulated curve compares very well to the experimental growth curves of EAhy926 cells (Figure 9B), obtained when cells are cultured as described in the Section 2. Both curves exhibit a typical sigmoid shape including three

different stages: a latency phase, followed by an exponential growth phase before reaching a plateau phase, indicating cell proliferation inhibition (Figure 9).

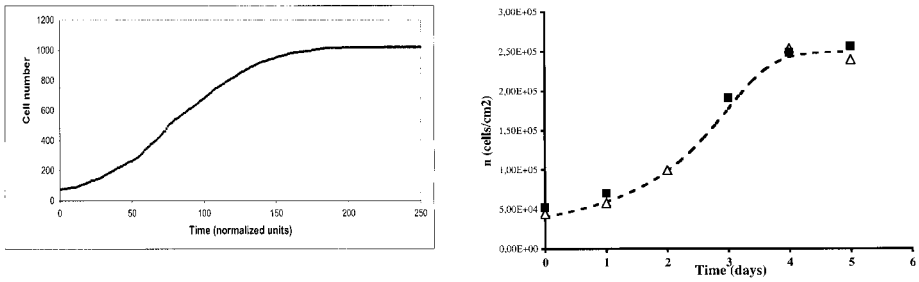

Figure 9. A: Increase of cell number by proliferation as given by the multi-agent model in the simulation of an IWH assay. B: Experimental growth curves obtained with the EAhy926 cell line in the experimental conditions given in Section 2. Two sets of experimental points are given. The dashed line indicates a fit to the experimental data obtained by a logistic-like model of cell proliferation.

4. DISCUSSION

This work provides a refined analysis of the migratory properties of the endothelial tumour cell line EAhy926. Precise quantification of such migration parameters in absence of imposed extracellular stimuli is indeed largely missing, even if this cell line is often used in experimental assays, especially those focusing on chemotaxis and tumour invasion (Albini *et al.*, 2000). Moreover, this quantitative analysis, undertaken both at the individual and at the cell population levels, has been originally used as a basis for discussing these quantification results within a multi-scale simulation framework, which integrates the quantitative data obtained at each level.

At the individual cell level, we satisfactorily based the quantification of the EAhy926 random motility (or cellular diffusion) coefficient on the persistent random walk model. In particular, we do need to consider a time dependence of the cell migration phenomenological parameters (Bergman and Zygourakis, 1999). Experimental values for mean migration speed and persistence time in our conditions are similar to values reported in the literature (DiMilla *et al.*, 1992; Kouvroukoglou *et al.*, 2000). Nevertheless, the persistent random walk model does not take into account cell-cell interactions, like cell-cell collisions or cell-cell adhesion. Such interactions could be of course minimized if using very sub-confluent cell monolayers, i.e. low initial cell densities. In a similar way, the persistent random walk model does not take into account cell proliferation. Once again, this drawback can be minimized by considering cell trajectories only during the first hours of the experiments, before a significant increase of cell number, which could bias the quantification of cell migration.

However, if these two strategies are adapted when following individual cell trajectories, they provide a quantification of cell migration which is quite far from realistic biological situations, where for instance populations of cells, like endothelial cells, expand to colonize a wounded area. Thus, in addition to individual cell

migration analysis, collective migratory cell behaviour has been characterized from data derived from wounded EAhy926 cellular monolayers. After rescaling the variation of the wounded area by the initial wounded surface, identical shapes of the wound kinetics curves were obtained (Figure 4). Furthermore, this generic shape highlights an apparent regulation of the wound closure speed when both wound margins come closer. A possible explanation of these data could be postulated by considering that the cells at the wound margins respond in an autocrine (Shvartsman *et al.*, 2001) and/or paracrine way to a chemical signal released by wounded cells. Wounding can indeed induce specific cell responses, as shown for instance by Klepeis *et al.* (2001) who reported the existence of a retrograde calcium wave which can activate the wounding process in the early stages. Secreted factors, like the autocrine motility factor (Funasaka *et al.*, 2001), could also be involved in this regulation process. Additionally, mechanical factors, associated to pre-existing stresses within the initial confluent cell monolayer, could also come into play. After wounding, mechanical stress relaxation would thus occur within both cell margins. This contribution to the apparent wound margins motion will decrease with time in absence of cell proliferation, but this internal pressure will be sustained if cell proliferation is large enough.

In this context, the formulation of a multi-agent model is proved here to be a valuable tool for analysing such modifications of cell migration by combining hypotheses and data from both the individual and the population cell levels. Based on a two-dimensional agent-model, the respective influence of environmental constraints, like the available free space, as well as the balance between different cell adaptation strategies (enhancement or inhibition of cell migration versus enhancement or inhibition of cell proliferation) has been investigated. In the model, the influence of these different aspects of cell dynamics occurs mainly through a limitation of the number of empty locations existing in each cell neighbourhood.

Our future computational work will also include the influence of the extracellular substrate more precisely, in particular to see how cell migration can be controlled by the concentration and spatial distribution of adhesives peptides coated on rigid or elastic substrates. Indeed, some of our non reported experiments indicate that cell migration behaviour is modified when different cell culture media were used: serum proteins can adsorb on material surfaces and subsequently affect cell functions like adhesion and migration. Experiments by Chen *et al.* (2003) also indicated that cell proliferation and cell protrusive activity highly depends on the cell morphologies dictated by patterned substrates. Previous studies with extracellular matrix protein substrates at increasing concentrations have shown that the migration speed of cells are regulated in a biphasic manner (DiMilla *et al.*, 1993; Palecek *et al.*, 1997). This biphasic response is also observed when cells migrate on patterned surfaces with different microgeometries (Tan *et al.*, 2001). Endothelial cell migration on surfaces coated with cell adhesion peptides RGD and YIGSRG also exhibit a significant increase of the persistence of cell translocation, and thus of cell motility coefficient (Kouvroukoglou *et al.*, 2000). However, we must still keep in mind that 2D migration assays are dedicated to specific cell types as endothelial or epithelial cells which have to migrate over extracellular matrix, while 3D migration assays describe more realistically *in vivo* situations for migration of other cell types like fibroblasts or leukocytes (Vernon and Gooden, 2002). A similar comparison between quantitative

characterization of cell motility from either individual cell tracking or collective behaviour could then be undertaken, as exemplified by Dickinson *et al.* (1993).

Furthermore, in our migration assays models, we did not include cell spreading, which appears as an important parameter for wound closure in the absence of cell proliferation (Galiacy *et al.*, 2003; Addadi-Rebbah *et al.*, 2004). While such a parameter has been considered in recent continuous mathematical models of wound closure (Salva *et al.*, 2004), its incorporation into discrete multi-agents models remains largely to be investigated. In this context, a more precise analysis of the modulation of the apparent cell migratory properties by mechanical factors (individual cell elasticity (Bereiter-Hahn and Lüers, 1994), internal monolayer pressure) would require considering each cell-agent as a deformable object (Dugnolle *et al.*, 1998), possibly in the framework of physical-object-oriented simulations (Promayon *et al.*, 2003).

ACKNOWLEDGEMENTS

The authors acknowledge Jocelyne Clément-Lacroix for technical assistance and Dr. Xavier Ronot for his advice in designing the *in vitro* wound healing experiments. This work is founded by a grant "ACI Télémédecine" from the French Centre National de la Recherche Scientifique (CNRS).

REFERENCES

Addadi-Rebbah, S., S. Poitevin, N. Fourre, M. Polette, R. Garnotel and P. Jeannesson (2004). Assessment of the antiinvasive potential of the anthracycline aclacinomycin (Aclarubicin) in a human fibrosarcoma cell line. International Journal of Oncology 24: 1607-1615.

Albini, A., C. Marchisone, F. Del Grosso, R. Benelli, L. Masiello, C. Tacchetti, M. Bono, M. Ferrantini, C. Rozera, M. Truini, F. Belardelli, L. Santi and D.M. Noonan (2000). Inhibition of angiogenesis and vascular tumor growth by interferon-producing cells: A gene therapy approach. American Journal of Pathology 156: 1381-1393.

Benndorf, R., R.H. Boger, S. Ergun, A. Steenpass and T. Wieland (2003). Angiotensin II type 2 receptor inhibits vascular endothelial growth factor-induced migration and in vitro tube formation of human endothelial cells. Circulation Research 93: 438-447.

Bereiter-Hahn, J. and H. Lüers (1994). The role of elasticity in the motile behavior of cells. In: Akkas, N. (Ed.). Biomechanics of active movement and division of cells, NATO ASI Series. pp 181–229. Springer Verlag, Berlin.

Bergman, A.J. and K. Zygourakis (1999). Migration of lymphocytes on fibronectin-coated surfaces:temporal evolution of migratory parameters. Biomaterials 20: 2235-2224.

Boucher, A., A. Doisy, X. Ronot and C. Garbay (1998). Cell migration analysis after in vitro wounding injury with a multi-agent approach. Artificial Intelligence Review 12: 137–162.

Bouis, D., G. A. Hospers, C. Meijer, G. Molema and N.H. Mulder (2001). Endothelium in vitro: a review of human vascular endothelial cell lines for blood vessel-related research. Angiogenesis 4: 91-102.

Boyden, S.B. (1962). The chemotactic effect of mixtures of antibody and antigen on polymorphonuclear leukocytes. Journal of Experimental Medicine 115:451-460.

Chen, C.S., J.L. Alonso, E. Ostuni, G.M. Whitesides and D.E. Ingber (2003). Cell shape provides global control of focal adhesion assembly. Biochemical and Biophysical Research Communications 307: 355-61.

DiMilla, P.A., J.A. Quinn, S.M. Albelda and D.A. Lauffenburger (1992). Measurement of individual cell migration parameters for human tissue cells. AIChE Journal 38: 1092-1104.

DiMilla, P. A., J.A. Stone, J.A. Quinn, S.M. Albelda and D.A. Lauffenburger (1993). Maximal migration of human smooth muscle cells on fibronectin and type IV collagen occurs at an intermediate attachment strength. Journal of Cell Biology 122: 729-737.

Dickinson, R.B., J.B. McCarthy and R.T. Tranquillo (1993). Quantitative characterization of cell invasion in vitro: formulation and validation of a mathematical model of the collagen gel invasion assay. Annals of Biomechanical Engineering 21: 679-697.

Dugnolle, P., C. Garbay and P. Tracqui (1998). A mechanical model to simulate cell reorganisation during in vitro wound healing, Proceedings ESM'98, "Simulation Tools in Biology". pp. 333-347 SCS Europe, Manchester.

Edgell, C. J., C. C. McDonald and J. B. Graham (1983). Permanent cell line expressing human factor VIII-related antigen established by hybridization. Proceedings of the National Academy of Sciences USA 80: 3734-3737.

Fenteany, G., P.A. Janmey and T.P. Stossel (2000). Signaling pathways and cell mechanics involved in wound closure by epithelial cell sheets. Current Biology 10: 831-838.

Funasaka, T., A. Haga, A. Raz and H. Nagase (2001). Tumor autocrine motility factor is an angiogenic factor that stimulates endothelial cell motility. Biochemical and Biophysical Research Communications 285: 118-128.

Galiacy, S., E. Planus, H. Lepetit, S. Fereol, V. Laurent, L. Ware, D. Isabey, M. Matthay, A. Harf and M.P. d'Ortho (2003). Keratinocyte growth factor promotes cell motility during alveolar epithelial repair *in vitro*. Experimental Cell Research 283: 215-229.

Ingber, D.E. (2002). Mechanical signaling and the cellular response to extracellular matrix in angiogenesis and cardiovascular physiology. Circulation Research 91: 877-887.

Kiernan, B. W. and C. Ffrench-Constant (1993). Oligodendrocyte precursor (O-2A progenitor cell) migration; a model system for the study of cell migration in the developing central nervous system. Development, Supplement: 219-225.

Klepeis, V.E., A. Cornell-Bell and V. Trinkaus-Randall (2001). Growth factors but not gap junctions play a role in injury-induced Ca^{2+} waves in epithelial cells. Journal of Cell Science 114: 4185-95.

Kouvroukoglou, S., K.C. Dee, R. Bizios, L.V. McIntire and K. Zygourakis (2000). Endothelial cell migration on surfaces modified with immobilized adhesive peptides. Biomaterials 21: 1725-1733.

Lauffenburger, D.A. L.G. and Griffith (2001). Who's got pull around here? Cell organization in development and tissue engineering. Proceedings of the National Academy of Sciences USA 98: 4282-4284.

Maheshwari, G. and D.A. Lauffenburger (1998). Deconstructing (and reconstructing) cell migration. Microscopy Research Technology 43: 358-368.

Manes, S., E. Mira, C. Gomez-Mouton, R.A. Lacalle and C. Martinez (2000). Cells on the move: a dialogue between polarization and motility. IUBMB Life 49:89-96.

Mansury, Y. and T.S. Deisboeck (2003). The impact of "search precision" in an agent-based tumor model. Journal of Theoretical Biology 224: 325-337.

Palecek, S.P., J.C. Loftus, M.H. Ginsberg, D.A. Lauffenburger and A.F. Horwitz (1997). Integrin-ligand binding properties govern cell migration speed through cell-substratum adhesiveness. Nature 385: 537-540.

Planus, E., S. Galiacy, M. Matthay, V. Laurent, J. Gavrilovic, G. Murphy, C. Clerici, D. Isabey, C. Lafuma and M.P. d'Ortho (1999). Role of collagenase in mediating in vitro alveolar epithelial wound repair. Journal of Cell Science 112: 243-252.

Promayon, E., J.L. Martiel and P. Tracqui (2003). Physical-object-oriented 3D simulations of cell deformations and migration. In: Alt, W., M. Chaplain, M. Griebel and J. Lenz (Eds). Polymer and cell dynamics-Multiscale modeling and numerical simulations. pp. 125-138. Birkhäuser, Basel.

Ronot, X., A. Doisy and P. Tracqui (2000). Quantitative study of dynamic behavior of cell monolayers during in vitro wound healing by optical flow analysis. Cytometry 41: 19-30.

Salva, U., L.E. Olson and C.M. Waters (2004). Mathematical modeling of airway epithelial wound closure during cyclic mechanical strain. Journal of Applied Physiology 96: 566-574.

Shvartsman, S.Y., H.S. Wiley, W.M. Deen and D.A. Lauffenburger (2001). Spatial range of autocrine signaling: modeling and computational analysis. Biophysical Journal 81: 1854--1867.

Soll, D.R. and E. Voss (1999). Two-and three-dimensional computer systems for analyzing how animal cells crawl. In: Soll, D. R. and D. Wessels (Eds). Motion analysis of living cells. pp. 26-52. Wiley-Liss, London.

Tan, J., H. Shen and W.M. Saltzman (2001). Micron-scale positioning of features influences the rate of polymorphonuclear leukocyte migration. Biophysical Journal 81: 2569-2579.

Tranqui, L. and P. Tracqui (2000). Mechanical signaling and angiogenesis : the integration of cell - extracellular matrix couplings, Comptes Rendus de l'Académie des Sciences, Série III 322: 1-17.

Vailhé, B., X. Ronot, P. Tracqui, Y. Usson and L. Tranqui (1997). In vitro angiogenesis is modulated by the mechanical properties of fibrin gels and is related to β_v, β_3 integrin localization. In Vitro Cellular and Developmental Biology Animal, 33: 763-773.

Varani, J. and P.A. Ward (1978). A comparison of the migration patterns of normal and malignant cells in two assays systems. American Journal of Pathology 90:159-172.

Vernon, R.B. and M.D. Gooden (2002). New technologies in vitro for analysis of cell movement on or within collagen gels, Matrix Biology 21: 661-669.

Zahm, J.M., H. Kaplan, A.L. Herard, F. Doriot, D. Pierrot, P. Somelette and E. Puchelle (1997). Cell migration and proliferation during the in vitro wound repair of the respiratory epithelium. Cell Motility and the Cytoskeleton 37: 33–43.